Direct Evidence of the Competing Nature between Electronic and Lattice Breathing Order in Rare-Earth Nickelates

Jong-Woo Kim,[1,*] Yongseong Choi,[1] S. Middey,[2] D. Meyers,[3,†] J. Chakhalian,[4] Padraic Shafer,[5] H. Park,[6,7] and Philip J. Ryan[1,8]

[1]*Advanced Photon Source, Argonne National Laboratory, Argonne, Illinois 60439, USA*
[2]*Department of Physics, Indian Institute of Science, Bangalore 560012, India*
[3]*Department of Condensed Matter Physics and Materials Science, Brookhaven National Laboratory, Upton, New York 11973, USA*
[4]*Department of Physics and Astronomy, Rutgers University, Piscataway, New Jersey 08854, USA*
[5]*Advanced Light Source, Lawrence Berkeley National Laboratory, Berkeley, California 94720, USA*
[6]*Department of Physics, University of Illinois at Chicago, Chicago, Illinois 60607, USA*
[7]*Materials Science Division, Argonne National Laboratory, Argonne, Illinois 60439, USA*
[8]*School of Physical Sciences, Dublin City University, Dublin 11, Ireland*

(Received 26 June 2019; accepted 6 February 2020; published 26 March 2020)

Correlated electrons give rise to both exotic electronic and magnetic properties in rare-earth nickelates. Here we present evidence of the interfacial coupling between two nickelate systems, $EuNiO_3$ (ENO) and $LaNiO_3$ (LNO), with different electronic and magnetic properties but with compatible structural registry giving rise to an electrostructural transition, unobserved in each constituent. Nominally, LNO remains in a paramagnetic-metallic $R\bar{3}c$ phase while orthorhombic ENO undergoes antiferromagnetic and insulating transitions. However, the ENO/LNO heterostructure displays a uniform rotational symmetry set by an entwined interface. This leads to an anomalous reduction of bond disproportionation in the ENO layer through the metal to insulator transition and concomitantly charge disproportionation opens the gap accompanied by antiferromagnetic ordering. Our results resolve a long-standing question in the physics of rare-earth nickelates, herein demonstrating that charge and bond disproportionation are competing mechanisms for the charge localization process in the rare-earth nickelate system.

DOI: 10.1103/PhysRevLett.124.127601

Emergent properties in strongly correlated materials are often complex and not well explained by conventional theories [1]. The competing interactions between charge, spin, and lattice degree of freedom result in exotic phenomena such as superconductivity [1], multiferroicity [2], and metal-insulator transitions (MITs) [3]. Metal-insulator transition within the Mott-Hubbard criterion is a particularly important feature related to high-temperature superconductivity as well as for low power computing, sensors, and other electronic device applications [3].

It is well known that most of the rare-earth nickelates ($RNiO_3$, where R is rare earth) exhibit a temperature-driven MIT [4]. Although the nature of the MIT in $RNiO_3$ can be explained by various models, including the Mott-Hubbard mechanism [5–7], negative charge transfer [8–10], charge ordering [11,12], and spin density wave [13,14], a comprehensive understanding of its origin and the nature of the insulating state remains elusive.

The strong coupling between lattice and electronic behavior has recently led to a myriad of new phenomena in engineered film heterostructures [15,16]. In particular, lifting orbital degeneracy by preferential occupation of orbital states in these artificial structures can lead to the two-dimensionality (2D) behavior reminiscent of quasi-2D conductivity in the high-T_c cuprate systems [17]. Because of strong electron-electron coupling, $RNiO_3$ exhibits a non-Fermi liquid behavior with *bad metal* characteristics where the mean free path is below the semiclassical Mott-Ioffe-Regel limit [18]. Such rich and diverse properties result from the cooperation and competition of charge, orbital, and magnetic interactions combined with bandwidth effects related to octahedral rotation and distortion [19].

In the case of heavy rare-earth nickelates $RNiO_3$, the monoclinic distortion for the insulator phase leads to two different Ni sites through bond disproportionation [20]. The Ni-O distance of one site is similar to the length of the ionic bond (IB) and the other is close to the covalent bond distance. The origin of the insulating behavior for each site is realized within the site selective Mott transition model [6]. Here, each site exhibits different characteristics; one site adheres to the Coulomb U potential Mott picture and the other one to a typical band insulator model where the valence band is completely filled. Within this framework, the charge disproportionation (CD) or antiferromagnetism (AFM) is not crucial to the appearance of the insulating phase due to the large bond disproportionation.

As the size of the rare-earth ion gets larger, the Ni—O bond distance lies between ionic bond and covalent bond

regimes. The p-d hybridized band of the d^8 orbital with ligand hole ($d^8\underline{L}$) is placed across the Fermi level [4]. The MI transition introduces p-d band splitting via CD and AFM ordering driven by Fermi surface nesting. It also imposes a symmetry reduction to the monoclinic phase (bond disproportionation) similar to the site selective Mott transition but not as well defined as the heavy rare earth $R$$NiO_3$ [11].

$EuNiO_3$ is a member of the $R$$NiO_3$ series which exhibits 3 distinct phases: paramagnetic metal, paramagnetic insulator, and antiferromagnetic insulator [21]. By changing the amount of R-site doping with respect to the end member of the phase diagram, i.e., La, which shows only paramagnetic metallic behavior, the whole phase diagram can be effectively reproduced. In particular, half doping with La shows the behavior practically equivalent to $NdNiO_3$ [22]. In this Letter, we employed an artificial superlattice structure composed of $EuNiO_3$ (ENO) and $LaNiO_3$ (LNO) to study the spatially separated mechanism of the electron-electron correlated interaction that leads to insulating behavior. Here, we find that the CD initiated at the MIT reduces the bond disproportionation in the ENO, which is essential for the site selective Mott transition picture. This implies that both mechanisms are prevalent and unexpectedly compete, leading to an increase in charge localization and pushing the system toward the insulating phase.

A superlattice heterostructure of (4 u.c. ENO/4 u.c.LNO) $\times$ 4 (u.c. is pseudocubic unit cell) was grown epitaxial on the $(1\,1\,0)_o$ (orthorhombic notation) surface of a $NdGaO_3$ substrate using pulsed laser deposition [23] (details are included in the Supplemental Material [24]). The stoichiometrically similar but R-site disordered system, $Eu_{0.5}La_{0.5}NiO_3$, shows the MIT with AFM ordering and structural distortion around ~200 K similar to $NdNiO_3$. The underlying mechanism is understood as a charge transfer gap opening, driven by the bandwidth reduction due to Ni—O—Ni bond angle changes, as the average tolerance factor of Eu and La is comparable with Nd [8]. In the superlattice structure, however, the local bond angles are quite different between the layers so that the interplay of transport, magnetic structure, and electronic interactions are expected to behave quite differently from the R-site disordered system. Furthermore, while the single layer shows insulating behavior up to 5 layers [25] in the superlattice form, LNO shows metallic behavior without any transition when its thickness is more than 3 unit cells [26–29]. Strikingly, this 4×4 superlattice thin film exhibits a clear MIT around 90 K with 4 layers of LNO. This quasi-two-dimensional superlattice structure allows us to probe the microscopic response of each layer separately.

Transport measurement from the ENO/LNO superlattice film shows a MIT near 90 K in Fig. 1(a). This indicates that both layers become insulating below the transition. Soft x-ray resonant magnetic scattering was performed at the beam line 4.0.2 of the Advanced Light Source. The x ray was tuned to Ni L_3 and L_2 edges to obtain sensitivity to the magnetic scattering on the Ni site. Across the MIT, emergence of the $(\frac{1}{4}\,\frac{1}{4}\,\frac{1}{4})$ AFM reflection reveals the Ni E'-type magnetic ordering. The temperature dependence of the $(\frac{1}{4}\,\frac{1}{4}\,\frac{1}{4})$ order reflection is shown in Fig. 1(a). The magnetic intensity starts around ~90 K, consistent with the MIT temperature. The inset of Fig. 1(a) shows a lack of satellite peak intensity near the $(\frac{1}{4}\,\frac{1}{4}\,\frac{1}{4})$ reflection. The contrast of x rays scattered from AFM-ordered ENO layers and from LNO layers with a different magnetic ordering (or disorder) should produce satellite peaks around $(\frac{1}{4}\,\frac{1}{4}\,\frac{1}{4})$ AFM reflection. The absence of such satellites along L

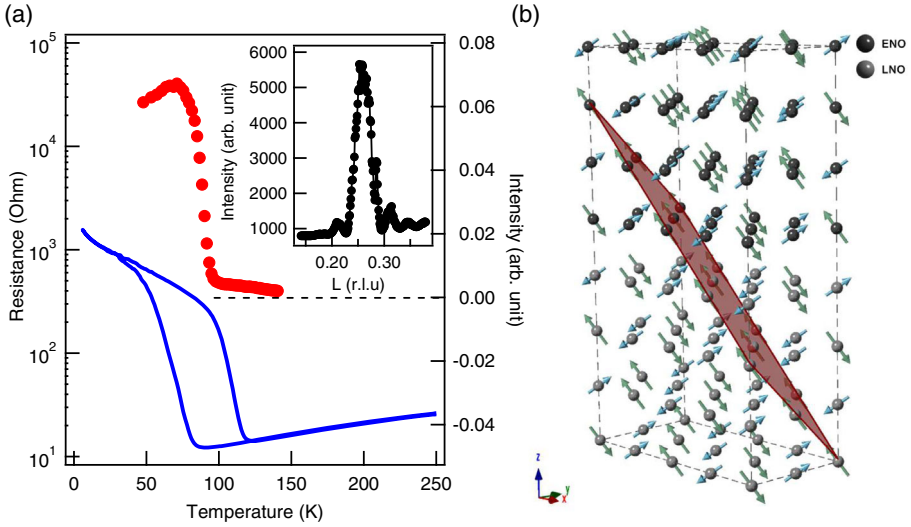

FIG. 1. (a) Temperature dependent resistivity (blue, left) and temperature dependence of $(\frac{1}{4}\,\frac{1}{4}\,\frac{1}{4})$ resonant soft x-ray magnetic reflection at the Ni L_3 edge (red, right). Inset: Reciprocal scan along surface normal (L direction). (b) The magnetic structure of the superlattice film showing 90° spin rotation with 4-unit-cell periodicity.

indicates no contrast in magnetic ordering between ENO and LNO.

Both MI and magnetic transitions in the LNO layer suggest a significant modification of its electronic behavior. Strong hybridization between the Ni d and O p orbitals and its sensitivity to structural distortion in the NiO_6 octahedra hints at likely changes in Ni-O local environments. Bulk ENO is reported as orthorhombic, but it is considered to be monoclinic below the MIT, while LNO is rhombohedral and is the only member of the $RNiO_3$ family without electronic, magnetic, and structural transitions. In order to resolve the symmetry of individual layers, x-ray diffraction was performed with a six-cycle diffractometer at the 6-ID-B beam line of the Advanced Photon Source. The x-ray energy was tuned to the Ni K edge to measure the resonance enhancement from the Ni CD order. The reciprocal L scan is carried out through the pseudocubic $(\frac{1}{2}\ \frac{1}{2}\ \frac{1}{2})$ film reflection [(101) in orthorhombic notation]. This peak is allowed for orthorhombic and monoclinic structures, but not for rhombohedral symmetry, and thus this structural contrast between layers should lead to satellite peaks. However, the absence of such satellite reflections indicates negligible contrast between the ENO and LNO layers. The ENO layers are highly tensile strained, so the out-of-plane lattice parameter is smaller than the bulk, leading to extensive oxygen octahedral distortion and rotation alongside accentuated R-site (Eu) displacements. The in-phase rotation along the orthorhombic c direction (Glazer notation c^+) is enhanced and propagates through the neighboring LNO layers. Sandwiched between ENO, the LNO layer is forced to adopt the $a^+b^-c^-$ rotation pattern of the adjoining ENO layers. This result clearly demonstrates how a heterostructured film enables interface engineering of an oxygen octahedral rotation pattern.

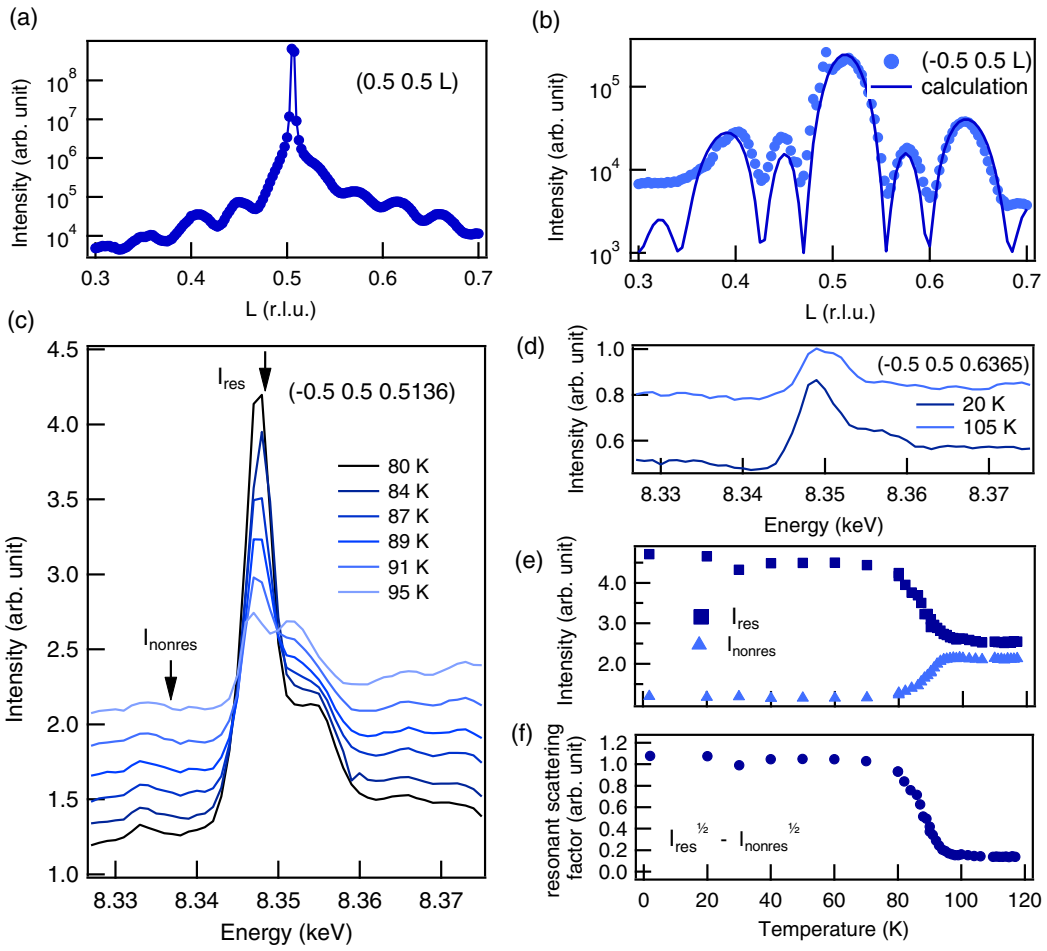

FIG. 2. (a) L scan through $(\frac{1}{2}\ \frac{1}{2}\ \frac{1}{2})$ reflection. (b) L scan through $(-\frac{1}{2}\ \frac{1}{2}\ \frac{1}{2})$ reflection. (c) Energy scans at the $(-\frac{1}{2}\ \frac{1}{2}\ \frac{1}{2})_{\mathrm{film}}$ reflection at various temperatures. The nonresonant intensity rises with the temperature increases while the resonant intensity decreases. (d) Energy scans at the superstructure satellite peak $(-\frac{1}{2}\ \frac{1}{2}\ +\frac{1}{4})_{\mathrm{film}}$ above and below the MIT. Because of the tail of the main resonant $(\frac{1}{2}\ \frac{1}{2}\ \frac{1}{2})$ reflection, the resonant component of Ni K edge slightly increases below the transition. (e) Temperature dependence of scattering intensities on and off resonance illustrating the contrast between charge ordering and charge disproportionation, respectively. (f) Temperature dependence of the resonant scattering factor obtained by $I_{\mathrm{res}}^{1/2} - I_{\mathrm{nonres}}^{1/2}$. Arrows in (c) indicated as I_{res} and I_{nonres} are the scattering intensities on and off resonant energies, respectively.

As reported previously, highly strained ENO exhibits octahedral breathing, which is related to monoclinic distortion [30]. This corresponds to a doubling of the unit cell, and therefore allows the $(-\frac{1}{2}\ \frac{1}{2}\ \frac{1}{2})$ reflection [$(0\,1\,1)$ in orthorhombic notation] which is forbidden in orthorhombic symmetry. The energy scan across the Ni K edge for this $(-\frac{1}{2}\ \frac{1}{2}\ \frac{1}{2})$ reflection shows some energy dependence due to off diagonal terms of the resonant scattering tensor [31] but does not exhibit a large resonant enhancement from the charge disproportionation as previously observed in $NdNiO_3$ and ENO/LNO superlattices [11,23]. The reciprocal L scan across the $(-\frac{1}{2}\ \frac{1}{2}\ \frac{1}{2})$ reflection measures the contrast between layers, examining whether the breathing structure has propagated into the LNO layers. Figure 2(b) shows the satellite peaks at $\pm 1/8$ position highlighting a contrast in the breathing mode distortion between the ENO and LNO layers. The LNO primarily maintains its orthorhombic structure with a suppressed monoclinic distortion while the ENO layers show monoclinic structure with large bond disproportionation 3(d). The characteristics of bonding states should be different between the ENO and the LNO layers, signifying two disparate ground states. It suggests that even though the ENO layer is insulating, LNO remains metallic, consistent with the observed metallic behavior at high temperatures.

The intensity of $(-\frac{1}{2}\ \frac{1}{2}\ \frac{1}{2})$ reflection and its satellites were measured to determine the extent of the monoclinic distortion. Upon cooling a reduction of the nonresonant intensity is observed through the transition; on the other hand, increasing the intensity at Ni K edge occurs due to CD. The energy dependence of the resonant profile is consistent with previous works [11]. No CD difference between ENO and LNO layers is detected from the satellite peak [Fig. 2(d)], which implies that the CD develops throughout the entire film.

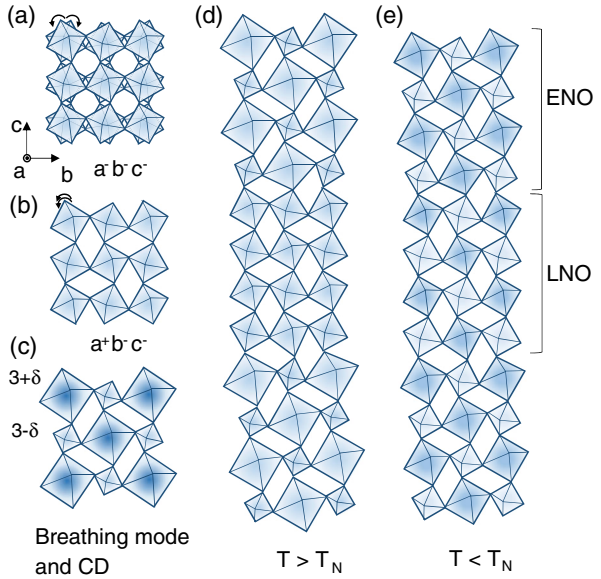

FIG. 3. (a) Octahedral rotation pattern of $a^-b^-c^-$. All a, b, and c are antiferrodistortive rotation axes (b) $a^+b^-c^-$ rotation pattern. The ferrodistortive axis is defined as the c axis of the orthorhombic unit cell. (c) Breathing mode and charge disproportionation. (d) Superlattice structure of breathing mode without CD and (e) with CD. The breathing distortion decreases with the CD.

The strong electron correlations in the $RNiO_3$ family affect the energy and occupancy of valence orbitals and thus induce the interdependence of charge, spin, and orbital degrees of freedom. Specifically, the insulating gap of the LNO layers is a representative example of such interdependence, as evidenced by the concomitant onset of CD and magnetic ordering. The near ionic state of the LNO layers drives the CD through the entire film by Fermi surface nesting across the metal-insulator transition. In a homogeneous $RNiO_3$, the octahedral breathing mode and CD often develop simultaneously. In contrast, for this ENO/LNO superlattice, the existing octahedral breathing structure of the ENO layers becomes less compatible with the emerging CD.

Here, we employ density functional theory plus dynamical mean field theory (DFT + DMFT) to study the interplay between the octahedral breathing mode and CD on the MIT in ENO. Calculations show that the bond length difference of the breathing amplitude is ~0.1 angstrom and the Ni—O long-bond site develops a Mott insulating state as the $d\ e_g$ occupancy is close to half (d^8). The short-bond (SB) site becomes a strongly covalent bonded band insulator ($d^8\underline{L}^2$) as the local moment in the SB site forms a singlet state with O hole spins. Based on this ground state structure, we simulate a structural modification of the breathing mode and an adjustment of d-p charge transfer energy for possible covalency change as a result of the structural change (details are shown in the Supplemental Material [24]). According to our calculations, simply modifying the structure to decrease the breathing mode amplitude (by 40%) does not increase the CD. On the contrary, it weakens the CD if it exists. The key factor is a reduction of covalency in Ni—O bonding. As the covalency lowers by increasing the d-p charge transfer energy, thus leaving the negative charge transfer regime, the CD grows significantly. Reducing the breathing mode amplitude leads to an increase of the SB length and a decrease of the covalency of the SB site Ni—O bonding. Therefore, the suppression of the octahedral breathing mode accommodates enhanced CD in the insulating phase.

For thinner LNO (<3 layers) in the $LaNiO_3/LaAlO_3$ superlattice, the magnetic order occurs at the MIT without obvious CD [29,31]. Instead, the insulating phase of the LNO can be driven by the spin density wave through the Fermi surface nesting due to the 2D confinement within the insulating layers. In contrast to dimensionality control, the electronic band structure of the LNO is tuned by the octahedral rotation pattern through the superlattice

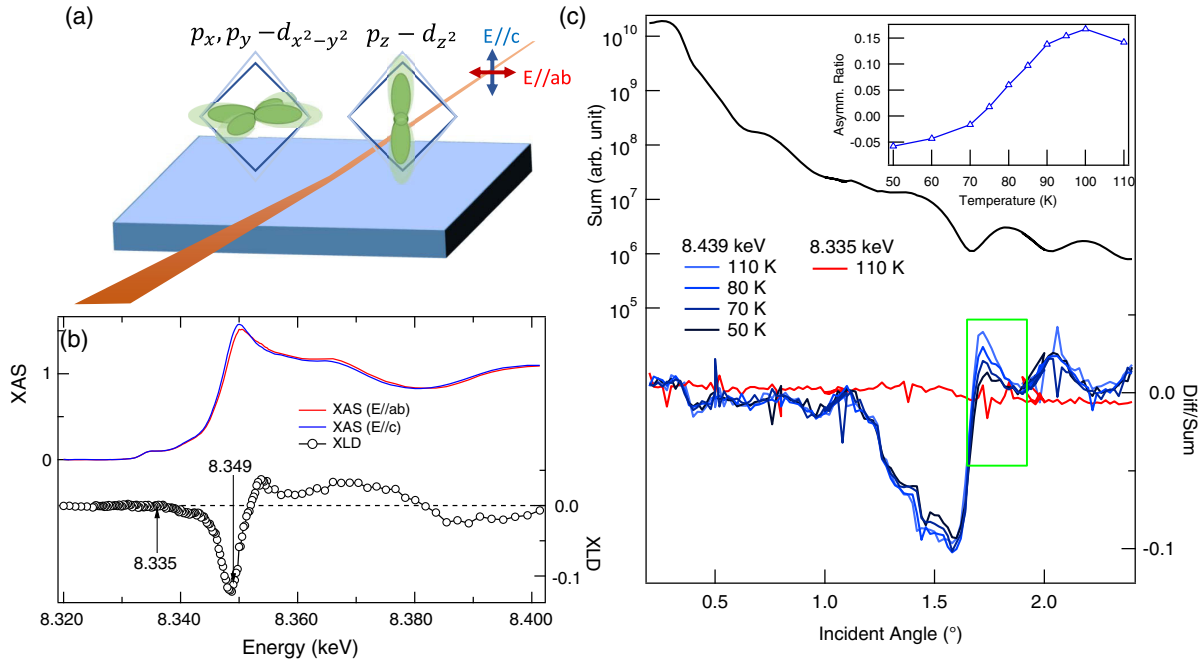

FIG. 4. (a) Illustration of x-ray resonant orbital scattering by switching between vertical ($E//c$) and horizontal ($E//ab$) polarizations with respect to Ni $3d$ and $4p$ orbital shapes. (b) X-ray linear dichroism (XLD) effects in x-ray absorption spectroscopy (XAS) across the Ni K edge. (c) Anisotropy in orbitals reflected in polarization dependent reflectivity, sensitive to the bilayer anisotropy contrast. Blue and red curves are taken at on- and off-resonant energies indicated by arrows in (b). Polarization dependence is plotted as difference divided by sum, with the difference and sum between two curves with polarization parallel and perpendicular to the surface normal direction. Inset: Temperature dependence for the sum of the polarization anisotropy within the energy range indicated by the green rectangular box. The orbital anisotropy decreases below the transition temperature.

arrangement of ENO/LNO. The configuration of the e_g orbital is tuned by a band level adjustment through interfacial interaction, as revealed by x-ray orbital reflectivity measurements taking advantage of the x-ray linear dichroism (XLD) [32]. We took a similar approach to probe the collective adjustment between the ENO and LNO layers across the MIT.

Utilizing the enhanced sensitivity with the parallel alignment between the incident polarization and probed orbital, XLD is a sensitive tool to study the anisotropies of the probed orbital states, as illustrated in Fig. 4(a). The incident polarization dependence of the Ni K-edge x-ray absorption spectroscopy (XAS) in Fig. 4(b) reveals anisotropic electronic environment around the central Ni ion in the NiO_6 octahedra. In the Ni K-edge XAS measurements, the Ni signals from the ENO and LNO layers are probed nearly uniformly due to a much larger probing depth (typically in microns) relative to the nanometer scale film thickness. As demonstrated in the orbital reflectivity study on the $LaNiO_3/LaAlO_3$ [32], grazing incident reflectivity can be implemented to enhance the bilayer contrast in orbital polarization. Similarly, we use the x-ray polarization dependence of resonant reflectivity in order to probe changes in the orbital occupation with temperature. Taking advantage of the enhanced bilayer contrast near the superlattice satellite peak, the layer contrast in XLD between ENO and LNO was measured by collecting the asymmetry ratio between the two reflectivity curves with orthogonal polarizations. While the similar layer thicknesses between the ENO and LNO layers suppresses the first order superlattice peak near 1.5° as shown in Fig. 4(c), the XLD difference between the two layers manifests as bilayer contrast. As shown in the inset of Fig. 4(c), this contrast gradually decreases with increasing CD below the MIT as the orbital occupation adjusts in order to accommodate the CD throughout the superlattice. This suggests that a synchronization of the Fermi surfaces occurs across the layers by the e_g orbital rearrangement opening an energy gap in the insulating state.

In conclusion, we present direct evidence of the competing nature between electronic charge ordering and bond disproportionation behavior across the MIT in an ENO/LNO heterostructure. Employing the superlattice design, we demonstrate structural accommodation between two dissimilar nickelate layers, lending itself as a promising platform to tune overall properties and to test theories underlying the observed phenomena. This leads to a way to achieve desired electronic properties by tuning competing interactions of charge and spin order in rare-earth nickelate systems.

X-ray diffraction and absorption experiments were carried out at beam lines 6-ID-B and 4-ID-D of the

Advanced Photon Source, Argonne National Laboratory, and at beam line 4.0.2 of the Advanced Light Source, Lawrence Berkeley National Laboratory. The work performed at the Advanced Photon Source was supported by the U.S. Department of Energy, Office of Science, and Office of Basic Energy Sciences under Contract No. DEAC02-06CH11357. This research used resources of the Advanced Light Source, which is a DOE Office of Science User Facility under Contract No. DE-AC02-05CH11231. S. M. acknowledges DST Nanomission Grant No. DST/NM/NS/2018/246 for financial support. J. C. is supported by the Gordon and Betty Moore Foundation EPiQS Initiative through Grant No. GBMF4534. H. P. is supported by the U.S. Department of Energy, Office of Science, Basic Energy Sciences, Materials Sciences and Engineering Division. We acknowledge the computing resources provided on Bebop, a high-performance computing cluster operated by the Laboratory Computing Resource Center at Argonne National Laboratory.

*jwkim@anl.gov
†Present address: Physics Department, Oklahoma State University, Stillwater, Oklahoma 74078, USA.

[1] D. Pines, Rep. Prog. Phys. **79**, 092501 (2016).
[2] D. I. Khomskii, J. Magn. Magn. Mater. **306**, 1 (2006).
[3] M. Imada, A. Fujimori, and Y. Tokura, Rev. Mod. Phys. **70**, 1039 (1998).
[4] M. L. Medarde, J. Phys. Condens. Matter. **9**, 1679 (1997).
[5] M. K. Stewart, J. Liu, M. Kareev, J. Chakhalian, and D. N. Basov, Phys. Rev. Lett. **107**, 176401 (2011).
[6] H. Park, A. J. Millis, and C. A. Marianetti, Phys. Rev. Lett. **109**, 156402 (2012).
[7] S. Johnston, A. Mukherjee, I. Elfimov, M. Berciu, and G. A. Sawatzky, Phys. Rev. Lett. **112**, 106404 (2014).
[8] J. B. Torrance, P. Lacorre, A. I. Nazzal, E. J. Ansaldo, and Ch. Niedermayer, Phys. Rev. B **45**, 8209(R) (1992).
[9] S. R. Barman, A. Chainani, and D. D. Sarma, Phys. Rev. B **49**, 8475 (1994).
[10] T. Mizokawa, D. I. Khomskii, and G. A. Sawatzky, Phys. Rev. B **61**, 11263 (2000).
[11] U. Staub, G. I. Meijer, F. Fauth, R. Allenspach, J. G. Bednorz, J. Karpinski, S. M. Kazakov, L. Paolasini, and F. d'Acapito, Phys. Rev. Lett. **88**, 126402 (2002).
[12] I. I. Mazin, D. I. Khomskii, R. Lengsdorf, J. A. Alonso, W. G. Marshall, R. M. Ibberson, A. Podlesnyak, M. J. Martínez-Lope, and M. M. Abd-Elmeguid, Phys. Rev. Lett. **98**, 176406 (2007).
[13] S. B. Lee, R. Chen, and L. Balents, Phys. Rev. Lett. **106**, 016405 (2011).
[14] M. Hepting, M. Minola, A. Frano, G. Cristiani, G. Logvenov, E. Schierle, M. Wu, M. Bluschke, E. Weschke, H.-U. Habermeier, E. Benckiser, M. Le Tacon, and B. Keimer, Phys. Rev. Lett. **113**, 227206 (2014).
[15] D. G. Schlom, L.-Q. Chen, X. Pan, A. Schmehl, and M. A. Zurbuchen, J. Am. Ceram. Soc. **91**, 2429 (2008).
[16] S. Middey, J. Chakhalian, P. Mahadevan, J. W. Freeland, A. J. Millis, and D. D. Sarma, Annu. Rev. Mater. Res. **46**, 305 (2016).
[17] J. Chaloupka and G. Khaliullin, Phys. Rev. Lett. **100**, 016404 (2008).
[18] R. Jaramillo, S. D. Ha, D. M. Silevitch, and S. Ramanathan, Nat. Phys. **10**, 304 (2014).
[19] J. B. Goodenough, Chem. Mater. **26**, 820 (2014).
[20] J. A. Alonso, J. L. García-Muñoz, M. T. Fernández-Díaz, M. A. G. Aranda, M. J. Martínez-Lope, and M. T. Casais, Phys. Rev. Lett. **82**, 3871 (1999).
[21] J. A. Alonso, M. J. Martínez-Lope, and I. Rasines, J. Solid State Chem. **120**, 170 (1995).
[22] R. D. Sánchez, M. T. Causa, A. Seoane, J. Rivas, F. Rivadulla, M. A. López-Quintela, J. J. Pérez Cacho, J. Blasco, and J. García, J. Solid State Chem. **151**, 1 (2000).
[23] S. Middey, D. Meyers, M. Kareev, Y. Cao, X. Liu, P. Shafer, J. W. Freeland, J.-W. Kim, P. J. Ryan, and J. Chakhalian, Phys. Rev. Lett. **120**, 156801 (2018).
[24] See Supplemental Material at http://link.aps.org/supplemental/10.1103/PhysRevLett.124.127601 for detailed information about film growth conditions and theoretical calculations.
[25] R. Scherwitzl, S. Gariglio, M. Gabay, P. Zubko, M. Gibert, and J.-M. Riscone, Phys. Rev. Lett. **106**, 246403 (2011).
[26] A. V. Boris, Y. Matiks, E. Benckiser, A. Frano, P. Popovich, V. Hinkov, P. Wochner, M. Castro-Colin, E. Detemple, V. K. Malik, C. Bernhard, T. Prokscha, A. Suter, Z. Salman, E. Morenzoni, G. Cristiani, H.-U. Habermeier, and B. Keimer, Science **332**, 937 (2011).
[27] J. Liu, S. Okamoto, M. van Veenendaal, M. Kareev, B. Gray, P. Ryan, J. W. Freeland, and J. Chakhalian, Phys. Rev. B **83**, 161102(R) (2011).
[28] J. Hwang, J. Son, J. Y. Zhang, A. Janotti, C. G. Van de Walle, and S. Stemmer, Phys. Rev. B **87**, 060101(R) (2013).
[29] A. Frano, E. Schierle, M. W. Haverkort, Y. Lu, M. Wu, S. Blanco-Canosa, U. Nwankwo, A. V. Boris, P. Wochner, G. Cristiani, H. U. Habermeier, G. Logvenov, V. Hinkov, E. Benckiser, E. Weschke, and B. Keimer, Phys. Rev. Lett. **111**, 106804 (2013).
[30] D. Meyers, S. Middey, M. Kareev, J. Liu, J. W. Kim, P. Shafer, P. J. Ryan, and J. Chakhalian, Phys. Rev. B **92**, 235126 (2015).
[31] Y. Lu, A. Frano, M. Bluschke, M. Hepting, S. Macke, J. Strempfer, P. Wochner, G. Cristiani, G. Logvenov, H.-U. Habermeier, M. W. Haverkort, B. Keimer, and E. Benckiser, Phys. Rev. B **93**, 165121 (2016).
[32] E. Benckiser, M. W. Haverkort, S. Brück, E. Goering, S. Macke, A. Frañó, X. Yang, O. K. Andersen, G. Cristiani, H.-U. Habermeier, A. V. Boris, I. Zegkinoglou, P. Wochner, H.-J. Kim, V. Hinkov, and B. Keimer, Nat. Mater. **10**, 189 (2011).